

An integrated field-numerical approach to assess slope stability hazards at volcanoes: the example of Pacaya, Guatemala

Lauren N. Schaefer · Thomas Oommen ·
Claudia Corazzato · Alessandro Tibaldi ·
Rudiger Escobar-Wolf · William I. Rose

Received: 2 October 2012 / Accepted: 14 April 2013
© Springer-Verlag Berlin Heidelberg 2013

Abstract Pacaya is an active stratovolcano located 30 km south of Guatemala City, Guatemala. A large (0.65 km³) sector collapse of the volcano occurred 0.6–1.6 ka B.P., producing a debris avalanche that traveled 25 km SW of the edifice. The current cone has since rebuilt within the scarp of this ancestral collapse. The structural setting of the volcano, along with two recent smaller-volume collapses in 1962 and 2010, suggests gravitational instability of this volcano. To assess Pacaya's stability and potential for another large lateral collapse of the active cone, standard engineering methodologies for studying non-volcanic slopes were used to examine the SW flank of the edifice. A geomechanical model was developed based on the physical–mechanical material properties of Pacaya's intact rocks and rock mass characteristics found through field observations and laboratory tests. Slope stability was analyzed in several scenarios with the Limit Equilibrium Method (LEM) and Finite Element Method (FEM), including static conditions (i.e., under gravity forces only), and considering the application of magma pressure and seismic force as triggering mechanisms for slope failure. Results show that the edifice remains stable under gravity alone; however, a large-scale collapse could be triggered by reasonable ranges of magma pressure (≥ 7.7 MPa if constant along a dyke) or

peak ground acceleration (≥ 460 cm/s²). Results also suggest that a layer of pyroclastics beneath the edifice could have controlled the ancestral sector collapse. Structural analysis shows that a transtensional stress regime is causing a NW–SE orientation of aligned features at the surface, and may be a controlling mechanism for the direction of a future collapse. FEM results are concordant with those from LEM and reveal that maximum shear strain patterns within the edifice may account for long lava flows erupted from lower vent elevations.

Keywords Volcanic slope stability · Limit Equilibrium Method · Finite Element Method · Pacaya volcano

Introduction

Volcanic landslides, which have caused over 20,000 fatalities in the past 400 years (Siebert et al. 1987), are extremely hazardous geologic processes due to their size and velocity. The largest events (sector collapses) can travel at speeds of 50 to 150 m/s (Ui et al. 1986; Siebert et al. 1995), emplacing several cubic kilometers of debris up to tens of kilometers away from the volcano. Geological and structural studies revealed that some volcanoes are prone to repeated lateral collapse events (see review in Tibaldi and Lagmay 2006). These events can be a serious threat to the conterminous areas, especially for those volcanoes that have suffered multiple collapse events in their history.

The past occurrence of catastrophic collapse, continual eruptive activity, and inherent geologic features of Pacaya volcano (Guatemala) demand an evaluation of potential future collapse hazards. Furthermore, Pacaya is surrounded

Editorial responsibility: S. A. Fagents

L. N. Schaefer (✉) · T. Oommen · R. Escobar-Wolf · W. I. Rose
Department of Geological and Mining Engineering and Sciences,
Michigan Technological University, Houghton, MI, USA
e-mail: lnschaeff@mtu.edu

C. Corazzato · A. Tibaldi
Dipartimento di Scienze dell'Ambiente e del Territorio e di
Scienze della Terra, Università degli Studi di Milano-Bicocca,
Milano, Italy

by several communities totaling approximately 9,000 people within 5 km of the active cone, and which have been evacuated 11 times in the past 24 years (Matías Gómez 2009). A collapse of the active cone would greatly expand the hazard zones; therefore, it is critical to understand the factors affecting slope stability. Recently, standard engineering methodologies for studying non-volcanic slopes using geomechanical models have been applied to studying volcanic slopes (see del Potro and Hürlimann (2008) and references therein). However, numerical data on the relevant mechanical properties remain a major source of uncertainty due to the lack of direct measurements (Thomas et al. 2004; del Potro and Hürlimann 2008). This paper investigates the possibility of merging different techniques in the field and laboratory to better characterize rock mass behavior for slope stability evaluation. We report new geological, structural, rock mechanical and geotechnical data on Pacaya. These data are integrated with laboratory tests to better define the physical–mechanical rock mass properties. Finally, these data are used in numerical models for the quantitative evaluation of lateral instability of large sector collapses and shallow landslides.

Background

Tectonic setting

Pacaya is an active stratovolcano in the Central American Volcanic Arc, associated with the subduction of the Cocos tectonic plate beneath the Caribbean plate (Fig. 1a). Regionally, the study area is located south of the active Motagua and Polochic left-lateral fault zones on the Caribbean tectonic plate, which is subjected to about 8 mm/year of crustal extension (Burkhart and Self 1985; Guzman-Speziale 2001; Lyon-Caen et al. 2006; Franco et al. 2012). This has formed a series of north-striking grabens, including the Guatemala City Graben (GCG), which presently absorbs most of the E–W extensional deformation. Additionally, this area is split by the WNW-striking right-lateral strike-slip Jalpatagua fault zone (JFZ), which has a slip rate of 10–14 mm/year (Carr 1976; Lyon-Caen et al. 2006; Franco et al. 2012). Pacaya is situated at or near the intersection of the GCG and the JFZ on the south rim of the Amatitlán caldera (Fig. 1a, b). The exact location and width of the JFZ are not well defined, but the available geologic maps for the area (IGN and Eggers 1969; Eggers 1972; Carr 1976; IGN and Bonis 1993) show a system of faults that run parallel to the main (and most obvious) topographic expression of the fault trace, and which if projected would intersect Pacaya to the NW.

Evolution of the Pacaya complex

Pacaya is a volcanic complex composed of several cones with a maximum elevation of 2,500 m above sea level (asl), described by four major phases proposed originally by Eggers (1972) and modified by Bardintzeff and Deniel (1992) as follows: (1) an ancestral andesitic volcano which is heavily eroded and capped with pyroclastics from the Amatitlán caldera; (2) the initial cone comprised of large lava flows, dated to about 0.5 Ma; (3) the emplacement of the Cerro Chino scoria cone and Cerro Grande and Cerro Chiquito domes on the NE flank about 0.16 Ma; and (4) the modern post-collapse MacKenney cone (Fig. 1b). Sometime between 0.6 and 1.6 ka B.P., the SW sector of the initial cone failed in a major edifice collapse, forming a debris avalanche that traveled 25 km SW and contained about 0.65 km³ of debris (Kitamura and Matías Gómez 1995; Vallance et al. 1995). This event left a large arcuate scarp whose western side is covered by younger lava, within which the modern cone was constructed (Fig. 1b) through historical times up to the present. After intermittent activity in the nineteenth century, Pacaya entered a period of repose (Feldman 1993). Activity renewed in 1961 and has since loaded lava flow and tephra material totaling a thickness of 100 to 150 m, primarily on the SW flank of the cone. This formed the active MacKenney cone (Fig. 1b), with the most recent activity occurring in 2010. The post-collapse cone is predominately composed of interbedded lava, breccia, and pyroclastics (mainly tephra fall and spatter). There are no significant petrographic differences between the prehistoric, historic, and modern lavas, which consist of porphyritic basalt with olivine and plagioclase phenocrysts (up to 45 wt%) and microphenocrysts, and minor clinopyroxene and magnetite microphenocrysts (Bardintzeff and Deniel 1992; Matías Gómez et al. 2012). Further details of the edifice's physical properties are described in Schaefer (2012) and references therein.

Factors contributing to slope instability and failure

Several factors at Pacaya can be considered potentially hazardous to the edifice's stability. One is a thick (10 to 200 m) sequence of tephra and ignimbrite layers that was deposited over the region prior to the formation of the initial cone (Fig. 1b; Eggers 1972; Wunderman and Rose 1984; Vallance et al. 1995). The local stratigraphy below Pacaya is poorly constrained, but from regional studies (e.g., Wunderman and Rose 1984) we can assume that this stratigraphy is dominated by these ignimbrites, tephra fall deposits, and volcanoclastic deposits reworked by secondary processes. The presence of a weak basal layer beneath a volcanic edifice such as this is considered a strong control on spreading and deformation that could eventually lead to

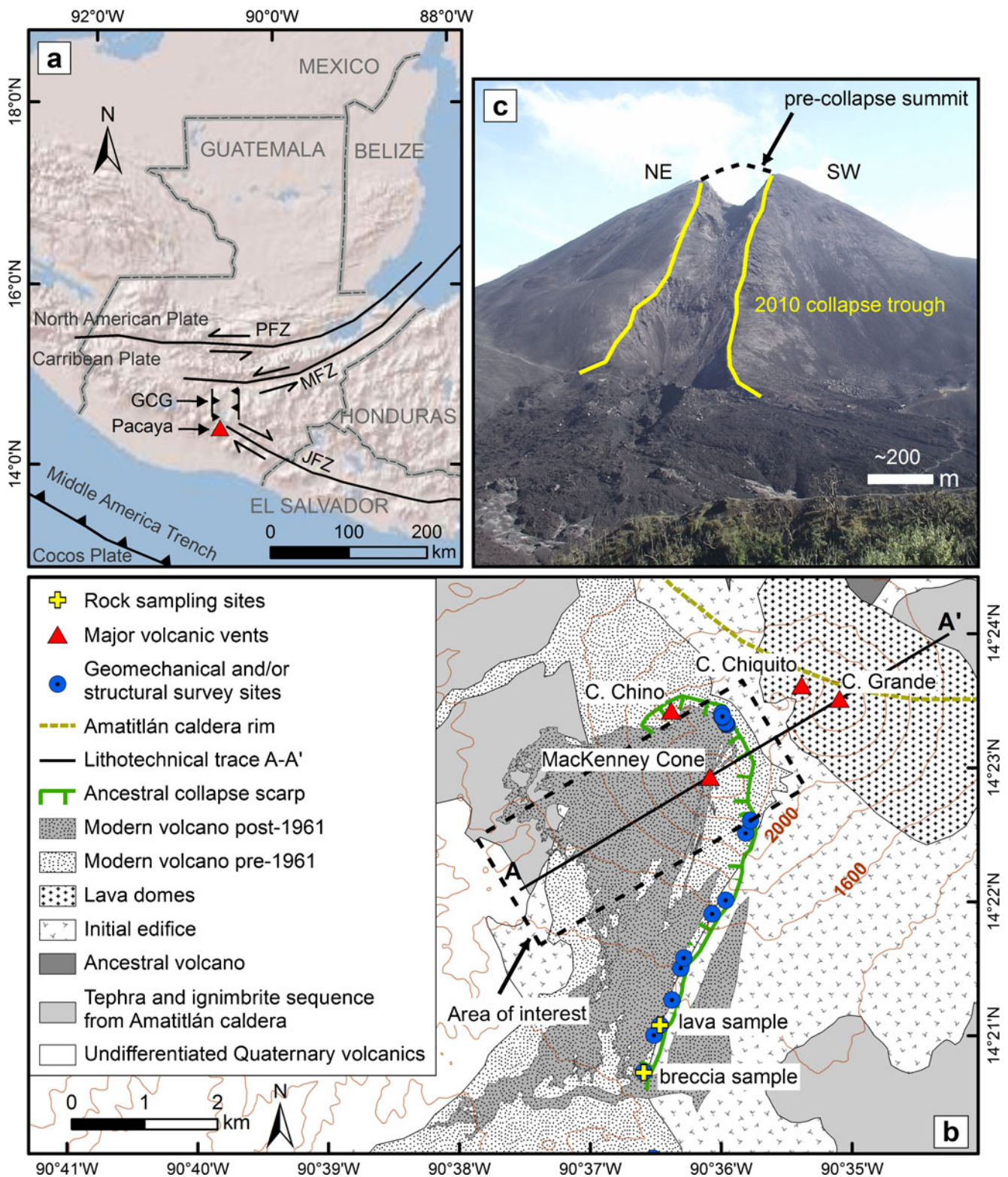


Fig. 1 Location of Pacaya volcano and main geologic and structural features. **a** Pacaya is located just south of the intersection of the right lateral Jalpatagua fault zone (JFZ) and the Guatemala City Graben (GCG) extensional zone. To the north are the Polochic (PFZ) and the Motagua fault zones (MFZ), which separate the Caribbean from the

North American tectonic plates (modified from Burkhart and Self (1985) and Lyon-Caen et al. (2006)) **b** General geology, modified from IGN/Eggers (1969) and Bardintzeff and Deniel (1992) **c** Collapse trough on the NW side of the MacKenney cone from 2010 eruptions

slope failure (Borgia et al. 1992; Merle and Borgia 1996; Delcamp et al. 2008). For example, the presence of a basal pyroclastic layer was noted as a factor inducing edifice collapse at Bandai volcano (Nakamura 1978).

Another consideration is that Pacaya is constructed over a south-sloping substrate (Vallance et al. 1995). Modeling by Wooller et al. (2004) demonstrated that volcanic collapse is more likely to occur in the direction of regional slope. For Pacaya, this would be to the southwest, which is the direction of the ancestral collapse and of current lava accumulation. Additionally, because the MacKenney cone has been built within the scarp of an old edifice, the north side is acting as a buttress. In analog modeling, asymmetry was demonstrated to enhance flank instability on the side with a lack of confinement, i.e., the southern side of Pacaya (Norini and Acocella 2011). As discussed above, geological and structural studies revealed that some volcanoes are prone to repeated lateral collapse events (see review in Tibaldi and Lagmay 2006), so the ancestral collapse could increase the possibility of another large collapse in the future.

An additional factor is the recent coincident summit Strombolian eruptions, collapse features, and flank lava eruptions that suggest the possibility of a magma reservoir high in the cone, an idea that has been hypothesized previously (Eggers 1983; Vallance et al. 1995; Matías Gómez 2009). The existence of a magma chamber shallow enough to cause subsidence high in the cone has serious hazard implications for collapse events, lateral or otherwise, as a larger eruption could cause significant changes in the cone shape, leading to collapse. This shallow magma chamber could have been an influencing factor in 1962 when an oval-shaped area, 300 by 200 m, subsided near the summit. This event followed the eruption of a long lava flow from a vent at the base of the cone only months before (see “1961 vent” in Fig. 2). This depression has since been filled with material from later eruptions. During eruptions in May 2010, a second collapse occurred when a linear trough developed on the NW side of the cone during eruptive activity (Figs. 1c and 2). This collapse trough, which is approximately 50–80 m deep and 100 m wide, extends 600 m from the summit. The exact timing of the trough formation is not known, but it seems to have happened between a large explosive eruption on May 27, 2010 and the eruption of a large lava flow on the SE of the Pacaya complex a few days later. This large lava flow erupted from a series of vents outside the ancestral collapse scarp, making these the first vents to erupt outside the scarp since the nineteenth century or earlier (see “2010 vents” in Fig. 2).

The origin of the collapse trough is not clear, but plausible scenarios include either horizontal extensional faulting,

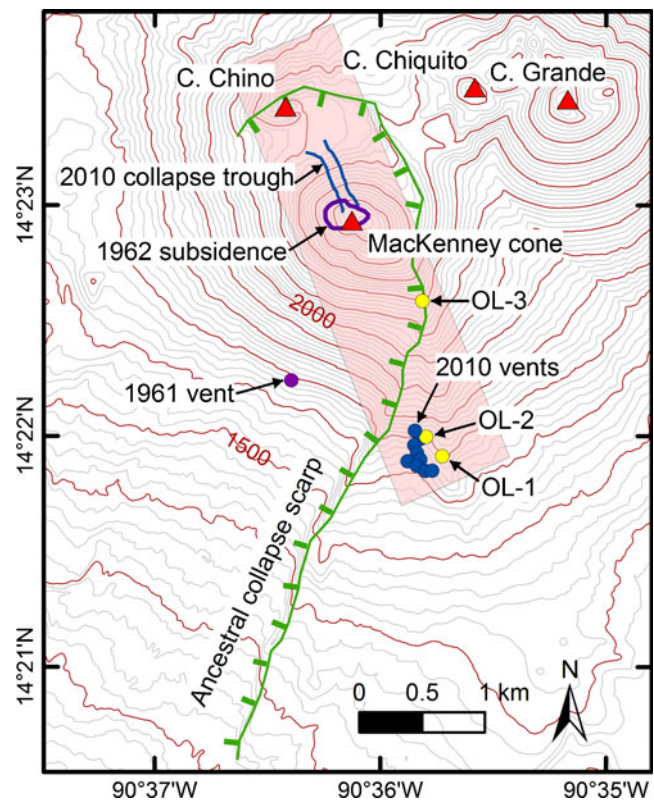


Fig. 2 Location of major vents and recent collapses suggests a preferential NNW orientation of magma ascent (shown by pink box), facilitated by the regional stress regime. The location of vents of older flows are marked by OL-1, OL-2, and OL-3

which formed a mini-graben, or vertical subsidence caused by magma withdrawal from within the edifice. In the first case, a substantial horizontal movement of the SW flank of the MacKenney cone would be implied, and in the second case, migration of a large volume of magma, perhaps to feed the effusive eruption to the SE, would be expected. Another possible mechanism of trough formation that cannot be completely ruled out is explosive excavation by a linear fissure-type vent during the most intense phase of the explosive eruption. The trough could also have formed by the opening of a vent at the base of the MacKenney cone at the NW end of the collapse trough. This could have caused subsequent landsliding and erosion of the loose cone material from upslope into the crater formed at the trough's distal end. We do not find any clear evidence for the latter two hypotheses and therefore prefer the first two as possible explanations. The combination of historic shallow collapses, the past occurrence of a catastrophic collapse, a layer of pyroclastics beneath the edifice, sloping basement substrate, buttressing of the edifice to the north, and recent asymmetrical accumulation of new material on a preexisting cone all increase the potential for slope failure.

Methodology and results

Structural analysis

We performed structural surveys to analyze brittle discontinuities, and additionally collected morphostructural data of volcanic features. The former were performed in the field to determine the local stress regime and most likely location of a potential slope failure. Along the scarp, fractures and joints were measured at the geomechanical survey sites (Fig. 3). The results for the brittle discontinuities indicate that both north-striking planes parallel to the regional grabens and NW-striking planes parallel to the Jalpatagua shear zone are reflected in the fracture and joint patterns measured along the scarp. Mapped fault orientations within 50 km from Pacaya (compiled from Carr 1976; IGN and Bonis 1993) also reflect the orientation of the main tectonic features so far described.

Morphometric analyses of volcanic features by field work and study of aerial photographs identified weakness zones possibly used as magma paths. Following Nakamura (1977), the orientation of fissures and the distribution of dykes and parasitic vents can be related to the state of the regional stress. A system of dykes radiating from a central conduit will tend to “bend” and align parallel with the direction of the (regional) horizontal greatest principal stress (σ_{Hmax}), or equivalently, perpendicular to the least principal stress (σ_3). In the case of Pacaya, the orientation of the trough formed during the May 2010 eruption is in a NNW

direction (Fig. 2). This orientation coincides with the opening of the new 2010 vent that formed on the SE flank of the volcano, and with older important vents, e.g., Cerro Chino, and the vents of older flows partially mapped by Eggers (1972) and re-mapped in this study based on aerial orthophotographs (OL-1, OL-2, and OL-3 in Fig. 2).

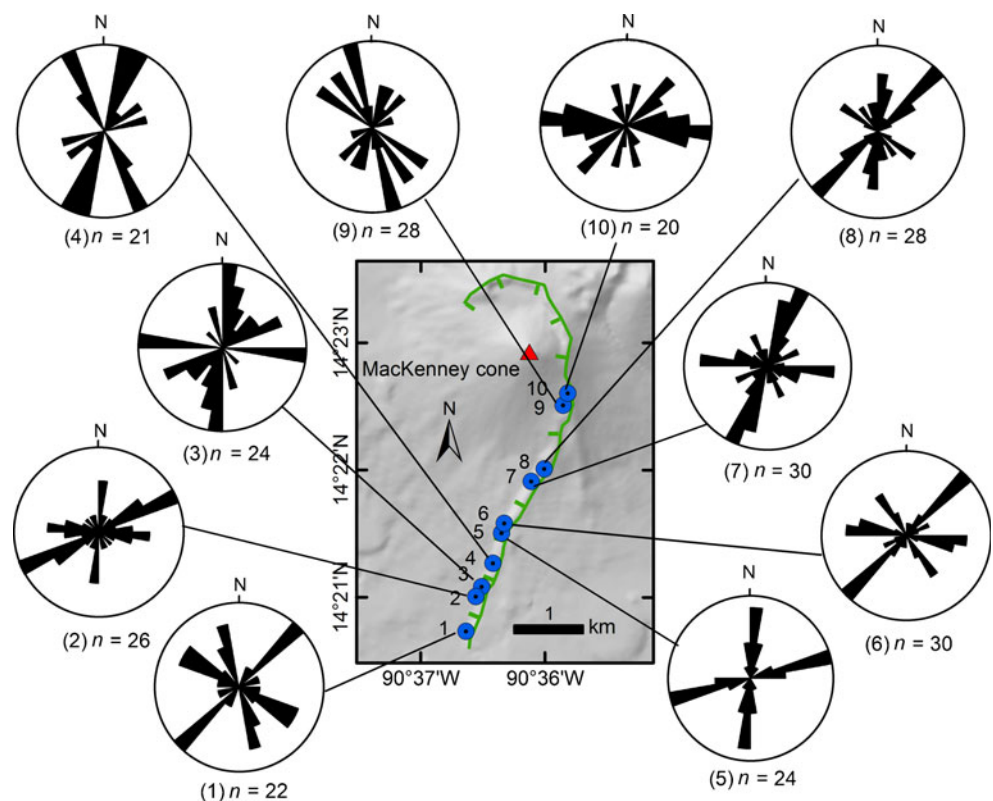
Nakamura (1977) also suggested that the elongation of volcanoes might reflect the regional state of stress parallel to the σ_{Hmax} . A volcano can grow under the influence of parallel feeder dykes and aligned vents, assuming an oriented elongation that coincides with the σ_{Hmax} . This also applies to Pacaya, as can be seen from the shape of the elevation contours (Fig. 2), which coincides again with the NNW orientation noted above. Moreover, the direction of the ancestral edifice collapse to the SW is almost perpendicular to the direction of cone elongation (NNW). This was observed at many other collapsed volcanoes worldwide (e.g., Moriya 1980; Siebert 1984; Tibaldi 2001), although several other factors may be contributing to the collapse orientation (e.g., Lagmay and Valdivia 2006; Siebert et al. 2006; Tibaldi et al. 2010).

Geotechnical analysis

Geotechnical model

Figure 4a shows a geological cross section of the volcano, with the geometry of the SW flank obtained from Digital

Fig. 3 Rose diagrams show the geometry of the joints and fractures at survey sites along Pacaya's scarp, with n being the number of joints and fractures measured



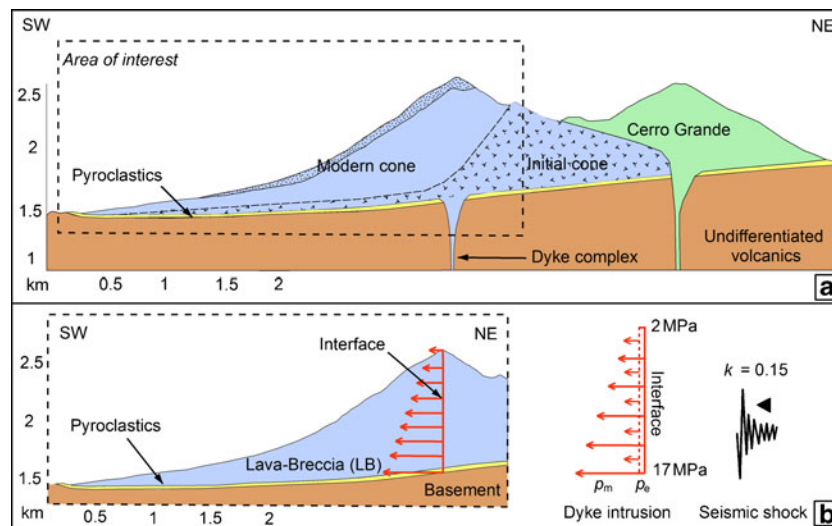


Fig. 4 Geological and geotechnical cross sections. **a** Geological cross section of Pacaya volcano with major geologic-structural features (trace *A-A'* in Fig. 1b). **b** Cross section showing lithotechnical units (lava-breccia, pyroclastics, and basement) and location of the physical interface representing the dyke, together with representation of external forces seismicity and magma pressure. Magma pressure components

include the magmastatic pressure (p_m) due to magma weight which increases with depth, and magma overpressure (p_e) which is constant along the interface height at 2 MPa. The area of interest is marked with a dashed box; however, the actual lower boundaries of the model are extended to avoid boundary effects during modeling

Elevation Models from 2001 (JICA et al. 2003). A geotechnical model of the volcano was then constructed for use in modeling using Limit Equilibrium (LEM) and Finite Element Methods (FEM; Fig. 4b). For numerical modeling purposes, geological units were simplified and categorized into lithotechnical units (Fig. 5a–d) according to their mechanical characteristics, based on field observations and geological maps, as follows:

1. Lava (L): predominately lava (>60 %) alternating with autoclastic breccia layers;
2. Lava+Breccia (LB): alternating lava (40–60 %) and breccia layers;
3. Breccia (B): predominately autoclastic breccia alternating with lava layers (<40 %); and
4. Pyroclastics (P): prevailing pyroclastics.

Although the material properties undoubtedly vary among these units and throughout the edifice due to rock and structural heterogeneity, the unknown distribution and lack of continuity of individual units require a simplification of the rock mass for the purpose of conceptual modeling. Pacaya has been characterized as having similar geochemical and petrologic properties throughout its growth (Eggers 1972; Walker 1989; Bardinezteff and Deniel 1992; Vallance et al. 1995). Therefore, the rock mass at Pacaya was grouped into the Lava–Breccia unit (LB), which represents the most prevalent percentage of lava to breccia in the studied outcrops (Fig. 5b). The rock mass properties for this unit are assumed uniform, representing an intermediate value of lava

and breccia rocks found through geomechanical surveys and tests performed along the collapse scarp (location given in Fig. 1b). Because the geometry of the ancestral collapse is unknown, an additional simplification is made in the modeling by not considering the possibility of a discontinuity between the post-collapse edifice and the modern cone, which could act as a zone of weakness and as a preferential fluid pathway (e.g., Frank 1995).

An additional complexity to the model involved the incorporation of the thick regional layer of dacite-rhyolitic tephra and ignimbrites. For the purpose of this work, we assume that the presence of a hypothetical layer of tephra and intercalated paleosols with an aggregated thickness of 30 m, similar to the exposed sequences that can be found to the north of the Amatitlán Caldera (Wunderman and Rose 1984). Since the mechanical properties of this pyroclastic material were not tested in the field, data from the literature for similar products were used (Thomas et al. 2004; Apuani et al. 2005a, b; del Potro and Hürlimann 2008). The LB unit and the layer of pyroclastics are modeled according to an elasto-plastic constitutive law. Analyses of the ancestral debris avalanche revealed no basement material in the deposit (Vallance et al. 1995); therefore, the edifice was modeled as sitting on top of a “basement” represented by undifferentiated volcanics, which was assumed to be a rigid body. In FEM analysis, boundary conditions on the sides of the model are fixed in both the “x” and “y” direction. A zoomed view of the model is shown in many figures (i.e., Fig. 4b, Fig. 7, Fig. 9, Fig. 10, and Fig. 11b) to display details

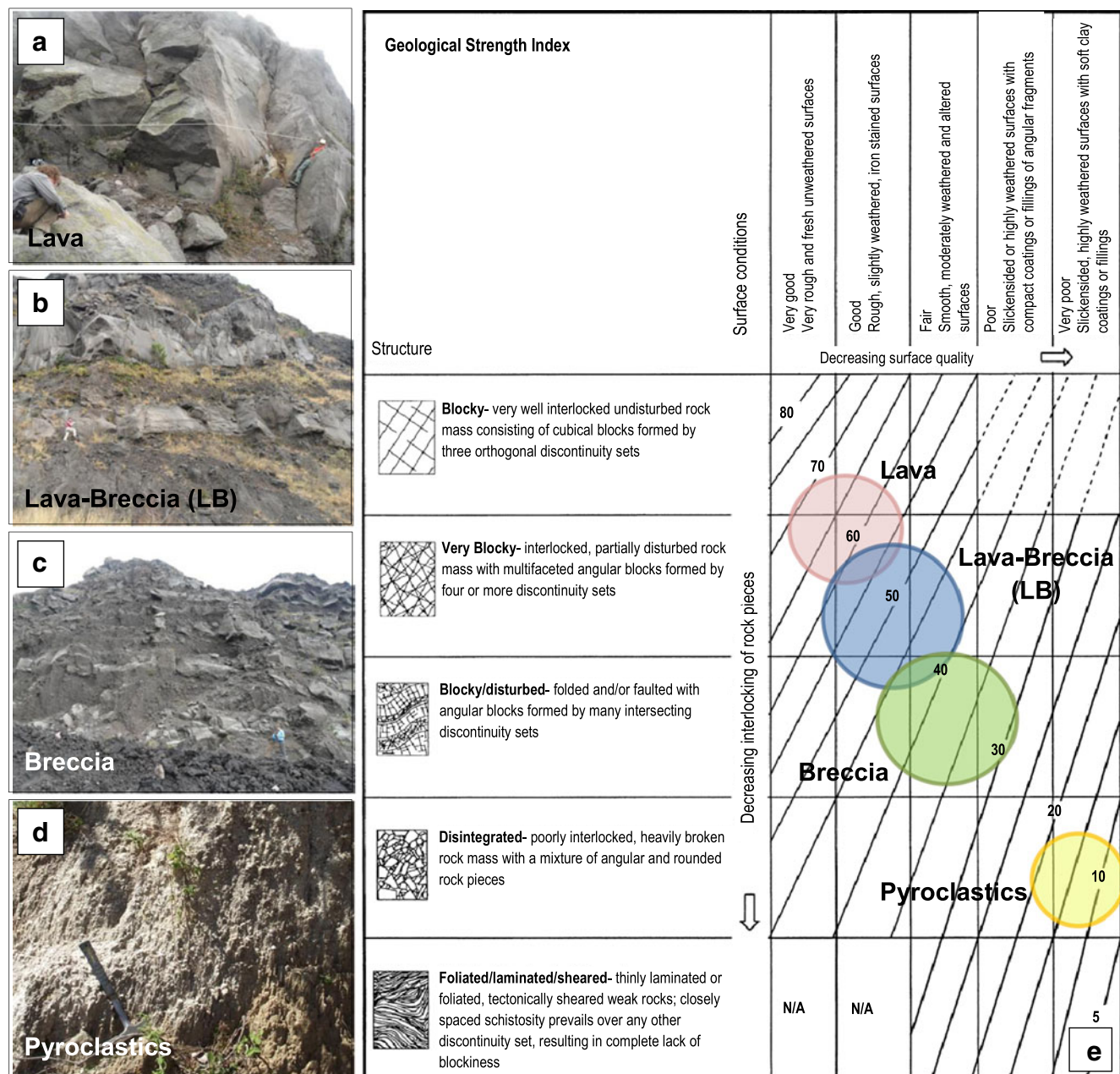


Fig. 5 Field-based rock mass characterization. **a–d** Four lithotechnical units were defined at Pacaya, based on the relative percentage of lava and breccia, or the presence of pyroclastic material: Lava, Lava-

Breccia, Breccia, and Pyroclastics. **e** Geological Strength Index (GSI) classification of the different lithotechnical units. Classification table modified from Marinos and Hoek (2000)

of the “Area of Interest” marked in Figs. 1 and 4. However, the lower boundaries were extended during modeling to avoid boundary effects. Data for the local water table are not available; therefore, all model conditions were considered dry.

Rock mass characterization

In order to provide a physical-mechanical dataset representative of a large volcanic edifice as a whole, it is fundamental to

couple the intact rock properties with the characterization of the rock mass geomechanical quality at outcrop conditions by evaluating the Rock Mass Rating values (Bieniawski 1989) and the Geological Strength Index (GSI, Hoek et al. 2002). The rock mass strength and deformability parameters at increasing confining stress are extrapolated by applying the Hoek–Brown failure criterion (Hoek 1994; Hoek et al. 2002), which enables the computation of the equivalent Mohr–Coulomb cohesion and friction angle as a function of the stress range of the analysis. The generalized Hoek and

Brown's non-linear strength law (Hoek et al. 2002) for jointed rock masses is defined by the equation:

$$\sigma'_1 = \sigma'_3 + \sigma_{ci} \left(m_b \frac{\sigma'_3}{\sigma_{ci}} + s \right)^a \quad (1)$$

where σ'_1 and σ'_3 are the maximum and minimum effective stresses at failure, σ'_{ci} is the uniaxial compressive strength of the intact rock, s and a are constants that depend upon joint conditions and the degree of fracturing for the rock mass expressed as:

$$s = \exp\left(\frac{\text{GSI} - 100}{9 - 3D}\right) \quad (2)$$

$$a = \frac{1}{2} + \frac{1}{6} \left(e^{-\frac{\text{GSI}}{15}} - e^{-\frac{20}{3}} \right) \quad (3)$$

The value m_b is a reduced material constant for the rock mass expressed as:

$$m_b = m_i \exp\left(\frac{\text{GSI} - 100}{28 - 14D}\right) \quad (4)$$

The GSI introduced by Hoek (1994) and developed by Marinos and Hoek (2000) uses visual characterizations of the rock mass structure and discontinuity surface condition. When combined with intact rock properties, the GSI can be used to extrapolate the rock mass strength and deformability parameters by applying the Hoek–Brown failure criterion. Using the GSI classification, the LB unit can be described by a good to fair surface quality and slightly disturbed structural integrity, which is a GSI value of 40–60 (Fig. 5e). The disturbance factor (D) is a numerical value of the degree of disturbance to which the rock mass has been subjected by blast damage, varying from zero (no disturbance) to unity (most disrupted). This disturbance factor originated from experience in the design of slopes in large mines, where the Hoek–Brown criterion tended to overestimate the rock mass strength (Hoek 2007). It is still unclear how to characterize volcanic rock masses in terms of D (Thomas et al. 2004); therefore, this study uses $D=0$ in considering the entire rock mass.

Another input parameter necessary for the Hoek–Brown criterion is the intact rock strength, which was measured in

the field using a Schmidt hammer. The Schmidt hammer measures the rebound of a spring-loaded mass impacting against the rock surface, which is hit with a defined energy. The rebound of the hammer is dependent on the hardness of the sample. The test was repeated 20 times at each survey site, and an average value was taken. These values were converted to equivalent uniaxial compressive strength (σ_{ci}) values using the following empirical correlation:

$$\sigma_{ci} = 2.75(N - 36.83) \quad (5)$$

obtained exclusively from testing volcanic rocks (Dinçer et al. 2004), with N being the Schmidt hammer rebound value. Using this relation, the uniaxial compressive strength is 88.03 ± 29.92 MPa for lava rocks (reported as average \pm standard deviation) and 47.6 ± 11.97 MPa for breccia rocks (Table 1).

The physical–mechanical properties summarized in Table 2 show the ranges and chosen input values (in brackets) used in numerical modeling, representing the predominate values found through field observations and laboratory tests. Laboratory uniaxial strength and bulk volume tests were completed by Manzoni (2012). Table 2 includes both the rock mass properties necessary for the Hoek–Brown failure criterion (Hoek 1994) and the calculated Mohr–Coulomb rock mass equivalent parameters that are typically used for LEM and FEM analysis. The generalized Mohr–Coulomb criterion describes a linear relationship between normal and shear stresses at failure and is described by:

$$\tau = c + \sigma \tan \varphi \quad (6)$$

where τ is the shear strength, σ is the normal stress, c is the intercept of the failure envelope with the τ axis and represents the cohesion, and φ is the slope of the failure envelope and represents the friction angle. In converting the Hoek–Brown to equivalent Mohr–Coulomb parameters, it is necessary to specify a range for the upper limit of confining stress ($\sigma'_{3\max}$) (Hoek et al. 2002). For Pacaya, this was calculated using Phase2 8.0 code (Rocscience 2011) using an empirical relationship considering the height of the slope and the unit weight of the rock mass, resulting in a range of $\sigma'_{3\max} = 5\text{--}15$ MPa. This is representative of the extent of the

Table 1 Uniaxial compressive strength (σ_{ci}) from Schmidt hammer and uniaxial compressive tests, and unit weight (γ) of volcanic samples

Sample	Schmidt hammer tests		Laboratory uniaxial tests		Unit weight	
	n	σ_{ci} (MPa)	n	σ_{ci} (MPa)	n	γ (kN/m ³)
Lava	18	88.03 \pm 29.92	12	47.62 \pm 16.01	17	26.82 \pm 0.11
Breccia	10	47.6 \pm 11.97	17	33.08 \pm 11.26	17	22.92 \pm 0.91

Values are given as the mean \pm the standard deviation, with n being the number of specimens tested

Table 2 Physical and mechanical properties of the lava-breccia (LB) and pyroclastics lithotechnical units

	Lithotechnical units	
	Lava-Breccia 40–70 % lava 30–60 % breccia	Pyroclastics Pyroclastic deposits
Intact rock, σ_{ci} (MPa)	52 S, Lb	10–20 (20) ^a
Geological Strength Index, GSI	45–60 (50) S	8–20 (15) S
Material constant, m_i	22±5 (22) Tr	13±5 (13) Tr
Disturbance factor, D	0 S	0 S
Unit weight, γ (kN/m ³)	25.65 Lb	8–20 (15) ^a
Mohr–Coulomb equivalent parameters calculated in the range $\sigma'_{3max}=5\text{--}15$ MPa		
Reduced material constant, m_b	3.689	0.625
Rock mass constant, s	0.004	0.0001
Rock mass constant, a	0.506	0.561
Apparent cohesion, c (MPa)	1.7–3.6	0.53–1.09
Friction angle, φ (°)	45.3–36.1	21.9–15.6
Tensile strength, σ'_{tm} (MPa)	–0.054	–0.003
Uniaxial compressive strength, σ_m (MPa)	3.132	0.1
Global strength, σ'_{cm} (MPa)	13.273	1.552
Young's Modulus, E_m (MPa)	3686	437

Laboratory analyses and results from Manzoni (2012)

S in situ direct tests and evaluations, Tr theoretical data, Lb laboratory results

^a Values from the literature (see text)

Values chosen for input in brackets when ranges are given

model at depth. The Mohr–Coulomb parameters were calculated using RocLab 1.0 (Rocscience 2011).

Slope stability analysis

Methodology

Volcano slope stability was analyzed with LEM using the Rocscience Slide 6.0 code. The outcome for the deterministic analysis is the Factor of Safety (FS), which is a ratio of the resisting and driving forces and describes the stability of the slope. Because of the presence of weak rocks and complex interior magmatic plumbing systems in volcanic

environments, the slope can be assessed as stable ($FS > 1.5$), moderately unstable ($1.3 < FS < 1.5$), inherently unstable ($1 < FS < 1.3$), or at failure ($FS < 1$) (Hoek 2007).

In this study, the stability of the volcanic slope was analyzed as a two-dimensional (2-D) plane strain problem. Previous studies have shown that this assumption provides lower estimates of stability and FS compared to three-dimensional (3-D) analyses (Michalowski 2010). Future studies would benefit from considering the 3-D effects to better constrain the out of plane extent and volume of potential slope instability.

Slip surfaces in LEM were calculated using the Janbu Simplified method. This method tends to be more

Table 3 Deterministic analysis trial conditions and outcomes

Input							Output	
Models	Pyroclastic unit?	Unit weight, γ (kN/m ³)	UCS, σ_{ci} (MPa)	Static	Magma pressure, p (MPa)	Seismic coefficient, k	FS	SRF
A-1	yes	25.65	52	x			1.81	1.99
A-2	no	25.65	52	x			2.55	2.79
B-1	yes	25.65	52		2–17 (top–bottom)		0.88	0.87
B-2	no	25.65	52		2–17 (top–bottom)		1.70	1.78
C-1	yes	25.65	52			0.15	1.20	1.32
C-2	no	25.65	52			0.15	1.94	2.15

Table 4 Sensitivity and probabilistic analysis inputs

Parameter	Unit	Mean	Standard deviation	Absolute minimum	Absolute maximum
Unit weight, γ : Lava-Breccia	kN/m ³	25.65	2.08	21.58	26.98
Uniaxial compressive strength, σ_{ci} : Lava-Breccia	MPa	52	23	35	140
Magma pressure (constant), p	MPa	9.5	–	0	24.56
Seismic coefficient, k	–	0.15	–	0	0.3

These values were assumed with a statistical distribution defined by the mean, standard deviation, and absolute minimum and maximum

conservative than others (Hung et al. 1989), which is justifiable for hazard assessments. The slip surface was not pre-defined, but found using an auto-refined, non-circular search method. This method uses an iterative algorithm to find the “global minimum” slip surface, or the surface with the lowest FS, and is suitable for considering irregular slip surfaces.

To follow stress and strain variations within the model when applying different disturbance factors (i.e., factors that influence the degree of disturbance in a rock mass), a 2-D FEM analysis was performed using the Phase2 8.0 code (Rocscience 2011). This 2-D elasto-plastic numerical model uses the Shear Strength Reduction method, which systematically reduces the strength parameters of a slope by a Shear Reduction Factor (SRF) and then computes the finite element stress analysis. This process is repeated for different SRF values until the deformations are unacceptably large, or the FEM does not converge to a solution within the specified tolerance. This determines the critical stage (i.e., instability) and the critical SRF value of the slope, a value equivalent to the FS (Rocscience 2011). Conclusions can be made by analyzing the “plasticization” of the model, which refers to a process of failure and fracturing in accordance with engineering mechanics. In particular, “plasticity indicators” show the zones in which the stresses satisfy the yield criterion. This type of analysis allows for a visualization of the development of failure mechanisms and eliminates the need for assumptions on the type, shape, and location of failure surfaces.

In both LEM and FEM analyses, models were evaluated in the following conditions:

- Model A: under gravity forces only;
- Model B: with magma pressure acting on a dyke;
- Model C: applying horizontal acceleration due to a seismic shock.

These were sub-grouped into models with a layer of pyroclastics (A-1, B-1, and C-1) and models without (A-2, B-2, and C-2), as outlined in Table 3. For each of these conditions, material properties were kept constant. The mean values for the material properties are given in Table 4. The same models and model properties adopted

for the LEM analyses were used in FEM analyses for direct comparison of the results.

For several parameters, LEM results were assessed using sensitivity and probabilistic analyses. Sensitivity analyses explore the effect on the FS due to variations in one parameter at a time within a range while keeping all the other variables constant. This assesses which parameters have the greatest influence on stability. Probabilistic analyses are performed to assess the probability of occurrence of a certain event (e.g., $FS < 1.5$), expressed by cumulative probability distribution functions. The inputs for these analyses were sampled with the Monte Carlo technique, with an assumed statistical distribution defined by the mean value, standard deviation, and absolute minimum and maximum values (Table 4).

Magma pressure (p) acting on a dyke includes the magmastatic component (p_m) and an excess-pressure (or overpressure) component (p_e) (Voight and Elsworth 1997):

$$p = p_m + p_e \quad (7)$$

Magmastatic pressure is a product of mean magma unit weight (γ_m) and height of the dyke (z). The value of magmastatic pressure increases with depth, reaching a maximum at the bottom of the edifice and grading to minimum to null at the summit. A mean magma unit weight of 22.56 kN/m³ was derived from the mean magma body density based on gravity studies at Pacaya by Eggers (1983). Assuming the dyke is 1,000 m high (extending from the base of the volcano to the summit), a maximum of $p_m = 22.56$ MPa can be calculated based on the following relation from Iverson (1995):

$$p_m = \gamma_m z \quad (8)$$

Following suggestions by other authors (Apurani et al. 2007; Apurani and Corazzato 2009), the maximum magmastatic pressure was reduced by 1/3 to $p_m = 15$ MPa for modeling. This accounts for situations that could reduce the pressure, such as magma moving through multiple conduits or changes in bulk density due to the presence of gaseous or solid phases.

Magmatic overpressure values for dykes feeding eruptions are not well constrained; however, Iverson (1995) suggested $0 \leq p_e \leq 10$ MPa as a reasonable range for excess magmatic pressure. This study adopted an excess pressure of 2 MPa that is applied as constant with depth in addition to the p_m values. This value is an estimate that falls within the range of the actual volcano behavior as recommended in previous studies (Rubin and Pollard 1987; Apuani and Corazzato 2009). The total magma pressure (p) values used in modeling ranged from 2 MPa for the top load to 17 MPa for the bottom load. For both LEM and FEM modeling, these values of magma pressure were applied as an outward-directed pressure on both sides of the “interface” surface. This simulates the presence of a magmatic feeding dyke extending 1,000 m from the base of the edifice to the main active vent at the summit (Fig. 4b). For sensitivity and probabilistic analyses, magma pressure was kept constant along the dyke interface.

To model the effects of earthquake loading in LEM and FEM analysis, a pseudo-static load was applied, which is a dimensionless coefficient that represents the maximum earthquake acceleration as a fraction of the acceleration due to gravity. A horizontal seismic coefficient (k) was applied as a body force directed out of the slope, or in the direction of failure. A recent seismic hazard analysis of Central America (Benito et al. 2012) gives a peak ground acceleration (PGA) range of 500 to 610 cm/s^2 with a return period of 500 years for the region where Pacaya is located. The horizontal seismic coefficient can be modeled as half PGA when expressed as a fraction of the gravitational acceleration (Hynes and Franklin 1984); therefore, a range of 0.25–0.3 appropriately describes the largest expected seismic event in the study area for a 500-year return period. To model a more probable earthquake event, or an earthquake with a lower return period, a lower value of 0.15 (PGA of 300 cm/s^2) was used for deterministic analysis.

LEM results

In static conditions, the SW flank is always stable ($FS > 1.5$). Sensitivity analysis shows that material properties would have to be increased (in the case of unit weight) or reduced (in the case of uniaxial compressive strength) to unrealistic values to induce the slope to fail under gravity alone (Fig. 6a, b). Both the uniaxial compressive strength (UCS), i.e., the capacity of a material to withstand axially directed pushing forces until the material fails, and the unit weight of the rock samples were considered. In model A-1, the UCS value for the LB unit would have to be reduced to 18.17 MPa (friction angle equivalency of 23.52°) for $FS = 1.5$, and 1.94 MPa (friction angle of 11.45°) for $FS = 1$, a reduction of 65 and 96 %, respectively, from the input values. These reductions are even greater in model A-2,

with UCS reduced to 11.4 MPa for $FS = 1.5$ and 0.64 MPa for $FS = 1$. Additionally, inputting a realistic range of unit weight based on laboratory tests, from 21 to 27 kN/m^3 , does not reduce the FS below 1.5. These values suggest that any reasonable change in material property values should not initiate a deep-seated landslide. However, magma pressure in a dyke can act as a destabilizing factor: if kept constant along the dyke, the slope reaches an unstable range ($FS < 1.5$) when magma pressure reaches 2.9 MPa, and failure ($FS < 1$) at 7.7 MPa in model B-1 (Fig. 6c). In model B-2, these pressures are 8.4 and 15.6 MPa, respectively. These values are well under the expected maximum of 17 MPa.

The inclusion of pyroclastics beneath the edifice greatly increases the depth of the potential slip surface and the amount of material predicted to fail (shown in Fig. 7a, b). This change in geometry is observed in all three models A, B, and C. The resulting failure surface in the models with a basal pyroclastic layer more closely resembles that of volcanic landslides elsewhere, which are described by Siebert (1984) as being deeper relative to the length of the depression, with high sidewalls and a gently sloping floor. This is in contrast to the shallower, spoon-shaped failure profiles of the models without the basal pyroclastic layer, which more closely resemble non-volcanic landslides (see comparison of volcanic vs. non-volcanic landslides, Fig. 5 in Siebert 1984). In all cases, the probability of the mass reaching instability is considerably higher in models that incorporate a layer of pyroclastics, as seen in the probabilistic analyses (Fig. 8). This emphasizes the effect that weak basal units can have on edifice stability.

Seismic acceleration can also cause the slope to become unstable. For model C-1, $FS < 1.5$ when the seismic coefficient reaches 0.06, and $FS < 1$ at 0.23 (Fig. 6d). Again, these values are well under the expected range of 0.25–0.3 for the maximum seismic coefficient. The seismic loading required to destabilize model C-2 without the pyroclastic unit is slightly higher than the expected maximum range, with $FS = 1$ at 0.31 and $FS = 1.5$ at values > 0.4 . This suggests that an earthquake capable of producing much larger accelerations would be required to destabilize the slope in this scenario, corresponding to a much longer return period, probably longer than 1,000 years (Benito et al. 2012).

Cumulative probability analysis shows that the probability of the slope reaching instability ($FS < 1.5$) is 90 % for model B-1 and 30 % for model B-2 if magma pressure is constant along the dyke interface (Fig. 8), the former being a considerably higher probability. In models where seismic force is applied, the mass reaches instability ($FS < 1.5$) with a probability of 78 % for model C-1, and of only 4 % for model C-2. The significance of these results lies in the difference between the models with and without a basal layer of pyroclastics. The cumulative probability values indicate

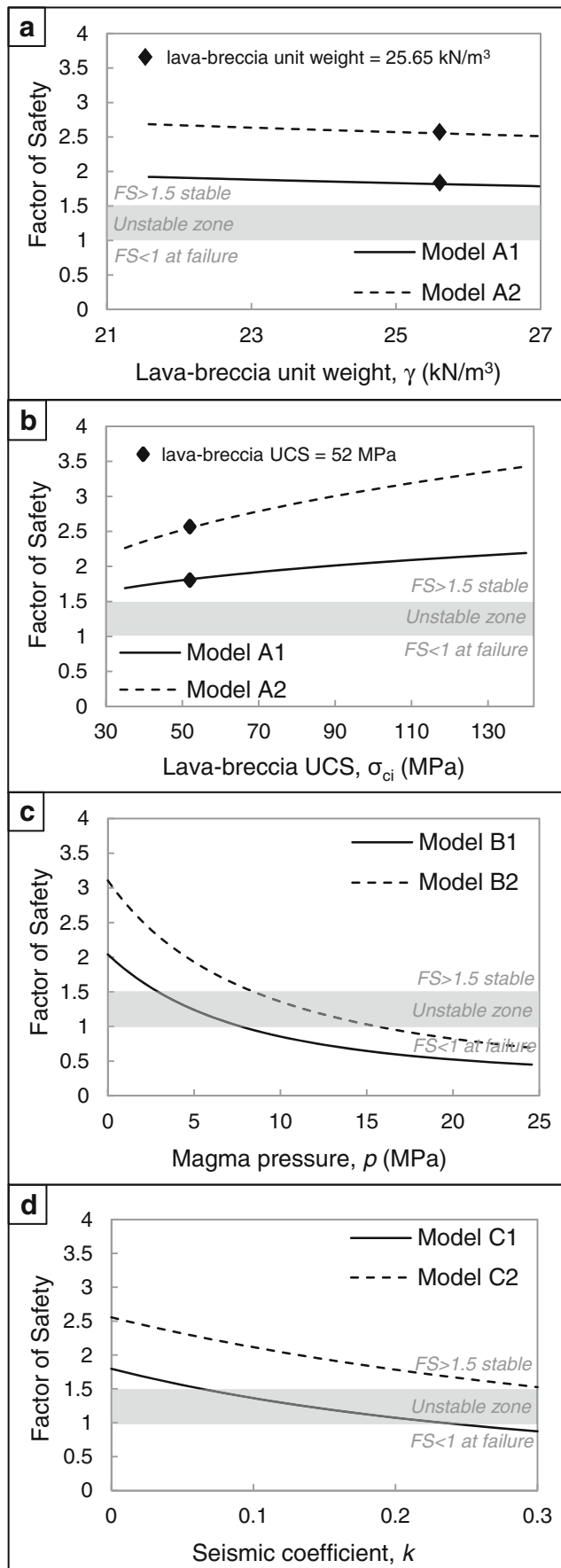


Fig. 6 Limit Equilibrium Method (LEM) sensitivity analysis results of several parameters, including **a** unit weight, **b** uniaxial compressive strength (UCS), **c** magma pressure if kept constant along the dyke interface, and **d** seismic coefficient. The UCS and unit weight of the lava-breccia unit would have to be changed to unrealistic values to induce failure. However, magma pressure in a dyke and seismic acceleration can result in instability ($FS < 1.5$) within expected ranges

that unless a weak layer exists beneath the edifice, the probability of these external triggers alone causing a large slope failure is relatively low.

FEM results

Unless otherwise stated, results discussed are for the critical SRF stage, which describes the point when results do not converge in FEM and the model reaches instability. The location of maximum shear strain within the edifice and the amount of displacement vary significantly for models with and without the basal layer of pyroclastics (Fig. 9a–h). For the models with a layer of pyroclastics, the area of maximum shear strain is concentrated within this layer and develops towards the surface at a steep angle (50°) during failure propagation (Fig. 9a, e). In contrast, models without a layer of pyroclastics tend to develop shallower areas of shear strain within the upper half of the cone (Fig. 9c, g).

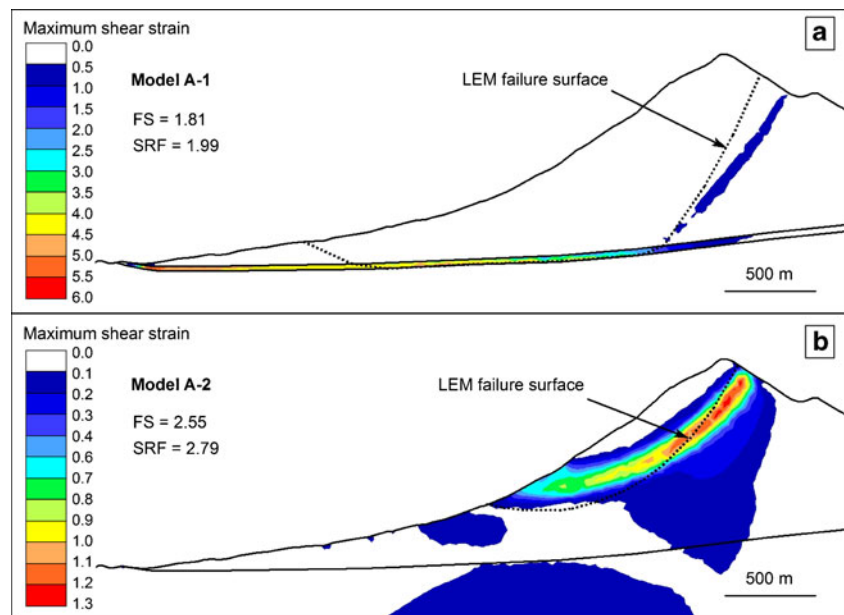
When magma pressure is applied, the shear strain in model B-1 is concentrated within the layer of pyroclastics and deformation (outlined in grey, Fig. 10) occurs as the edifice slides and spreads along this layer. In contrast, model B-2 develops deformation as a bulge in the middle of the cone that ultimately collapses (Fig. 10). The application of seismic acceleration produces areas of maximum shear strain and deformation patterns that are similar to those observed in models A and B. However, the models with seismic force have lower SRF values (Table 3) and higher shear strain and displacement values than models with a dyke intrusion (Fig. 9e–h).

Discussion

The lesson from the previous geological history

The previous history of the volcano allows predictions of the most plausible preferential direction of failure. The field geological-structural data indicate the presence of brittle discontinuities that strike N–S and NW–SE. Their strike and dip angle indicate that they are parallel to regional structures, comprising the north-striking Guatemala City Graben (GCG), and the NW-striking right-lateral strike-slip Jalpatagua fault zone (JFZ). The orientation of the GCG is consistent with an E–W-trending least principal

Fig. 7 Limit Equilibrium Method (LEM) critical slip surface superimposed on Finite Element Method (FEM) contours of maximum shear strain for **a** model A-1 and **b** model A-2. This change in geometry of the slip surface was also observed for models B and C. The unstable mass geometry outlined in the models with pyroclastics resembles the magnitude of the ancestral collapse, suggesting that the presence of pyroclastic deposits beneath the edifice could have been a controlling factor in the collapse. The presented shear strain represents one stage past the critical SRF to analyze the progression of failure and compare with the LEM failure surfaces



stress (σ_3), which is in turn consistent with the orientation of σ_3 along the JFZ. In concert, these features could indicate an ENE tensional component in a transtensional setting, perhaps resulting from the superposition of the right lateral shearing of the JFZ and the extension happening to the north of Pacaya, at the GCG. These inferences are compatible with research on the regional tectonic deformation and stress state in the area (Guzman-Speziale 2001; Caceres et al. 2005; Lyon-Caen et al. 2006; Álvarez-Gómez et al. 2008; Franco et al. 2012).

Our morphometric analysis of the orientation of past and recent volcanic craters and fissures indicates that the currently active MacKenney vent, the ancestral Cerro Chino vent, the new 2010 vents outside of the ancestral collapse scarp, and the 2010 trough feature are

all aligned in a NNW–SSE pattern (outlined by pink box, Fig. 2). We consider these aligned features as the expression of a weakness zone that favors magma upwelling to the surface. This volcanic rift zone is perpendicular to the regional ENE–WSW σ_3 ; thus, we consider that the geometry of the NNW-trending volcanic rift of Pacaya may be controlled by regional tectonics. Moreover, the SW orientation of the ancestral collapse may have been structurally controlled by the orientation of the NNW weakness zone.

If we take into consideration all of the structural features, the most likely direction of a future collapse is aligned roughly NE–SW. The large Cerro Grande and Cerro Chiquito lava domes on the NE flank of the volcano likely act as a buttressing agent and this, paired with recent loading of lava flow material on the SW flank of the MacKenney cone, suggests that the most likely direction for a possible future collapse will be to the SW. This inference is additionally supported by the N to S sloping regional basement (Vallance et al. 1995).

Slope stability evaluation

In studying the stability of the SW flank of the Pacaya volcano using LEM and FEM approaches, various destabilizing processes were considered. Sensitivity analyses show that weakened rock properties, such as a reduction of uniaxial compressive strength through hydrothermal alteration, are unlikely to induce a large-scale failure and landslide. This is especially true at Pacaya given the relatively young age of the edifice, making it unlikely that extensive hydrothermal alteration has occurred. Therefore, the slope is highly unlikely to have a catastrophic failure under gravity alone, unless affected by another mechanism.

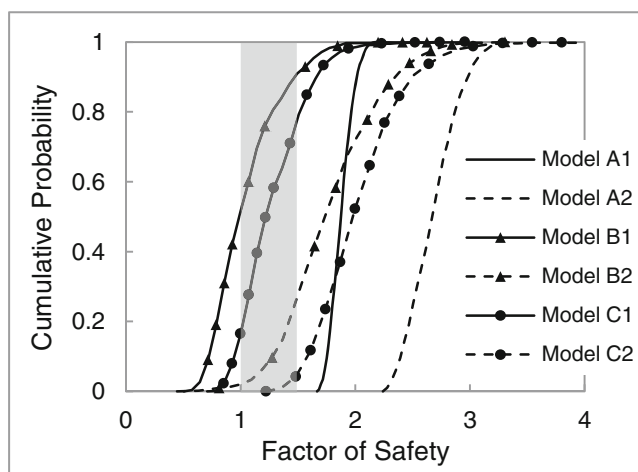


Fig. 8 Limit Equilibrium Method (LEM) cumulative probability of failure for each model condition. Magma pressure for the probability analysis is kept constant along the dyke interface. Unstable zone (Factor of Safety from 1 to 1.5) marked in grey

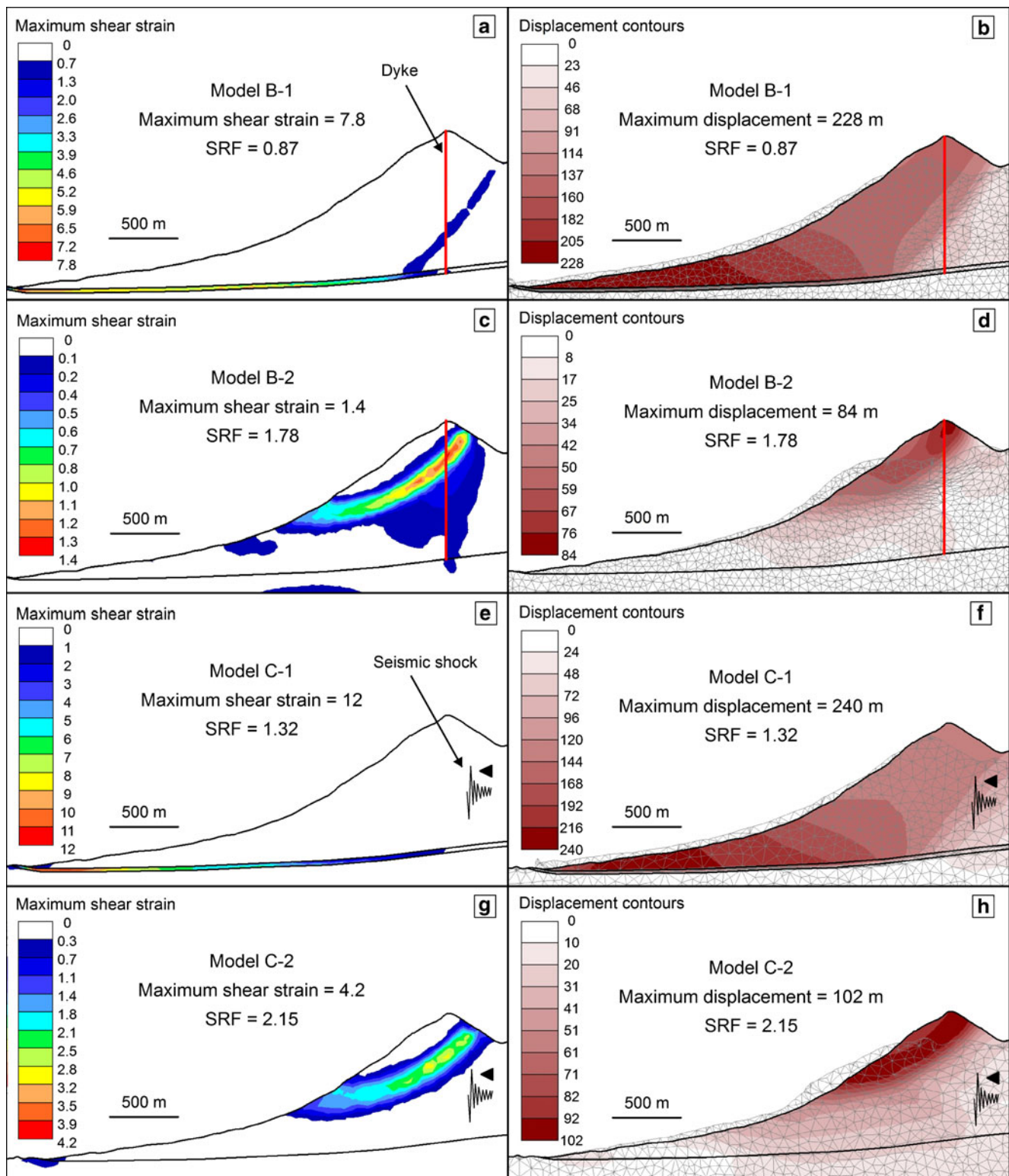


Fig. 9 Finite Element Method (FEM) results from the injection of magma (a–d) and application of seismic force (e–h). Results include both the location of maximum shear strain (left column) and the

location of displacement with the resulting deformation mesh (right column). The presented shear strain represents one stage past the critical SRF to analyze the progression of failure

However, the consistent LEM failure surface and FEM shear strain pattern through failure propagation for each model

condition (under gravity, magma pressure, and seismic forces) indicates that the material properties and geometry

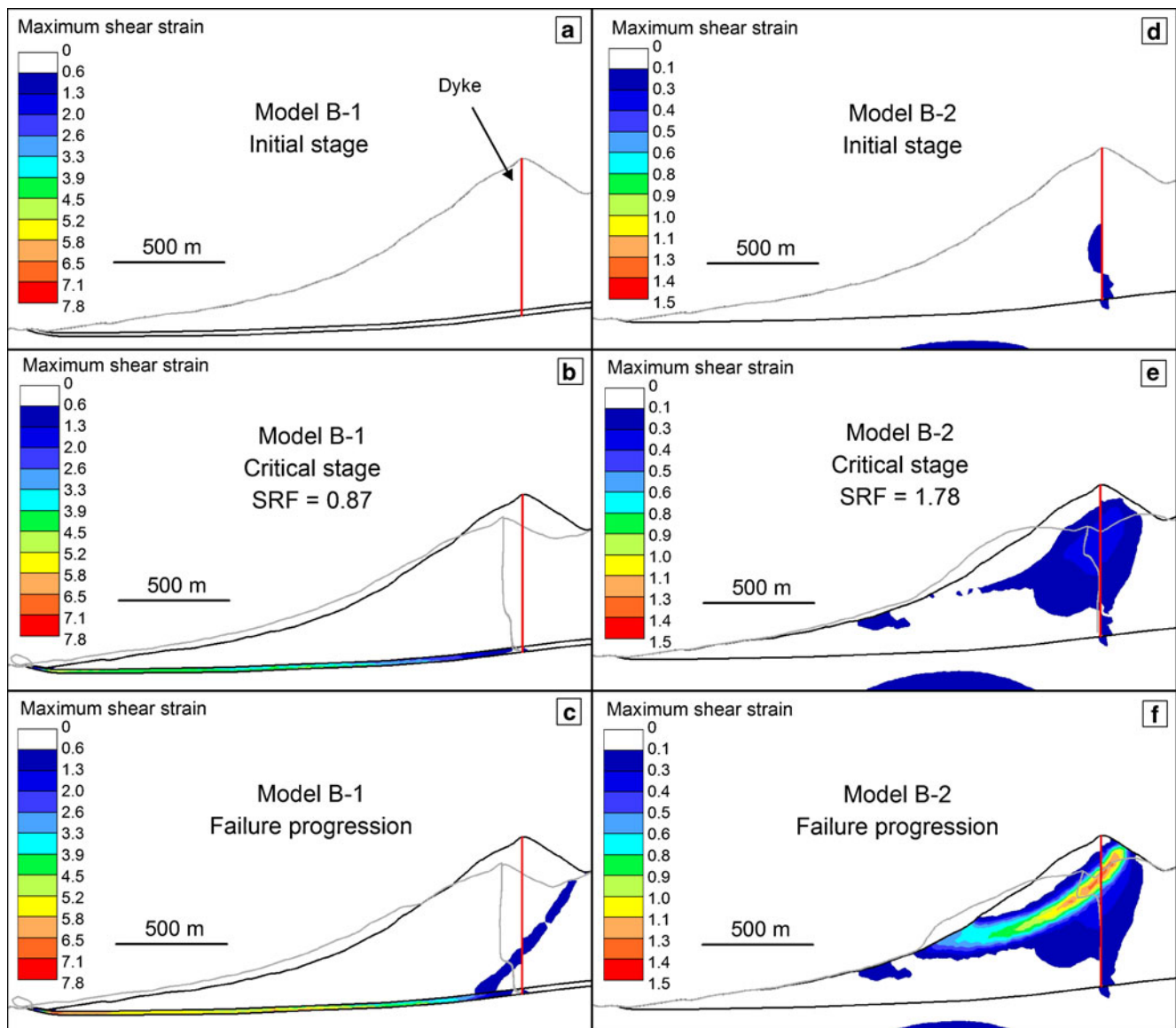


Fig. 10 Development of maximum shear strain within the edifice and deformation of the slope (in grey) during magmatic application. **a–c** A layer of pyroclastics beneath the edifice causes the cone to slide and spread along this layer, developing thrusts at the base of the edifice. **d–f** Without a basal layer of pyroclastics, deformation develops as a

concentrated bulge. Models are shown progressing through different stages of perturbation, from the initial stage with no magma pressure (*top*), to the critical SRF stage (*middle*), to the development of maximum shear strain during failure (*bottom*)

of the slope, and not the specific triggers, are the main factors controlling the failure geometry patterns.

Some models show that shear strain is concentrated at elevations around 1,600–1,800 m asl. This is the same elevation occupied by the 2010 vent and other older vents on the SW slope of Pacaya. Maximum shear strain zones can partially explain this trend as shear fractures can act as conduits for magma to drain out at lower vents (Fig. 11). The differences in the location of shear strain and types of displacements seen between the two model subcategories (1 and 2) in models A–C provide important insight into collapse behavior. If indeed

there is a layer of pyroclastics beneath the edifice, geodetic studies will likely show an overall deformation of the slope as the cone slides and spreads along this layer of pyroclastics, leading to the development of thrust faults at the base of the edifice (Fig. 10a–c). If this layer does not exist, or is not the controlling factor for collapse, deformation may develop as a concentrated bulge on the slope where the magma pressure is being applied within the edifice (Fig. 10d–f). This situation is similar to the cryptodome intrusion seen at Mount St. Helens (Moore and Albee 1981). This hypothesis merits further investigation.

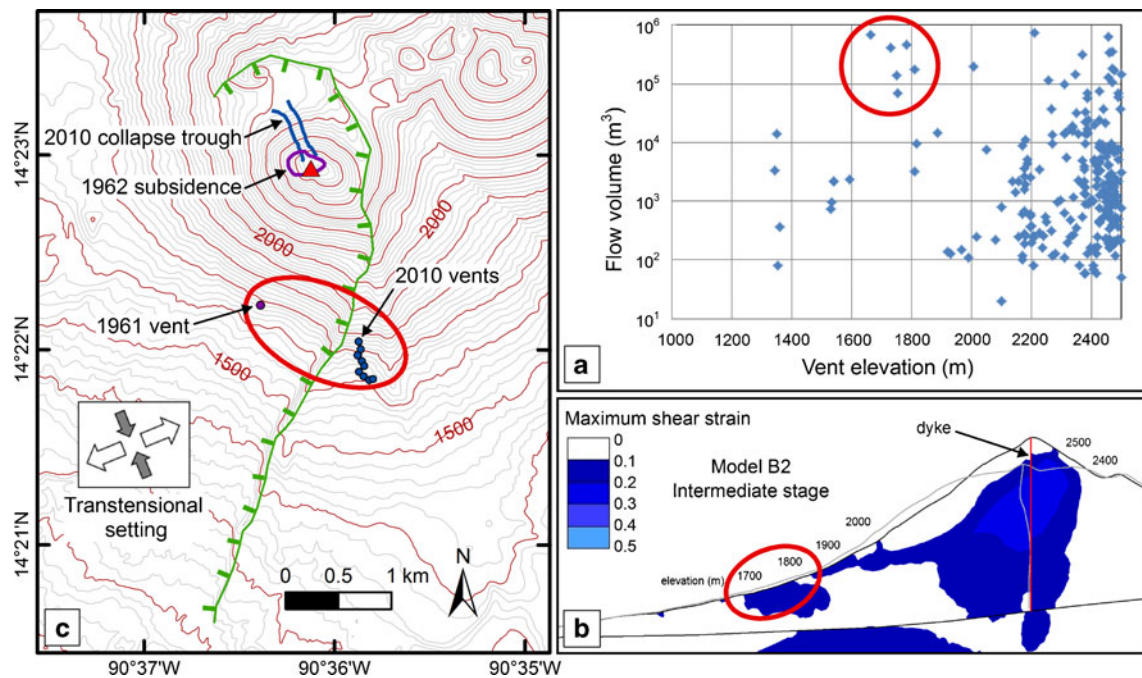


Fig. 11 Flank vent parameters and locations. Vents that have produced large lava flows ($1,000,000 \text{ m}^3$ or greater) are clustered at the top of the cone and at elevations of 1,600 to 1,800 m (circles in red). **a** Plot of lava flow volume vs. vent elevation modified from Matías Gómez et al. (2012). **b** Finite Element Method (FEM) analysis shows shear strain

patterns from 1,600 to 1,800 m asl during magma pressure application. **c** The vents that produced large lava flows are in this same elevation, suggesting that shear fractures are acting as conduits for magma to drain out at lower vents

Reasonable values of both magma pressure and seismic activity can destabilize the SW slope, with magma pressure having the strongest effect among the cases analyzed. Although the slope can fail in what is considered to be the unstable range ($1 < FS < 1.5$), values necessary to reach more definite slope failure ($FS < 1$) suggest that a larger magma intrusion (magma pressure $\geq 7.7 \text{ MPa}$ if constant along a dyke) or seismic event ($PGA \geq 460 \text{ cm/s}^2$) is needed to trigger a catastrophic collapse. The high values of maximum displacement in models B and C, ranging from 84 to 240 m, suggest that these triggers are capable of inducing displacements of large amounts of material. The current PGA values used to determine the horizontal seismic coefficient for the pseudostatic analysis are from a national study that has not considered possible local sources. Therefore, a more detailed seismic hazard analysis of local sources and site effects is needed to verify the PGA value at Pacaya. Additionally, the effects of ground deformation caused by fault rupture and movement from a potential seismic fault underneath the Pacaya edifice, e.g., an extension of either the strike-slip JFZ or extensional GCG normal faults, could also cause the collapse of the volcanic edifice; such possibilities have not been considered in this study.

The unstable geometry described by models incorporating a layer of pyroclastics (models A-1, B-1, and C-

1) resembles the mass that is expected of the large ancestral collapse, estimated at 0.65 km^3 of debris by Vallance et al. (1995). This suggests that the basal layer of pyroclastics could have controlled the ancestral failure, and could be an important controlling factor for a future collapse. Additionally, models with the layer of pyroclastics have a higher probability of reaching instability than those without. Therefore, it is important to better determine the mechanical properties of such hypothesized layers, and to obtain better estimates of their locations and thicknesses beneath the edifice. It is necessary to note that the MacKenney cone has not been reconstructed to the edifice's pre-failure configuration, hence the future collapse, although potentially quite large, might be expected to be of somewhat smaller volume. However, a collapse of this anticipated size would still cause a significant impact to settlements surrounding the volcano.

The presence of vents aligned across the Pacaya cone, defining a potential NNW–SSE structurally weak zone, indicates that dyke injection is a plausible geometry for the surface magma plumbing system, similar to those at Stromboli volcano or at Reunion Island (Corazzato et al. 2008; Bonali et al. 2011). Dyke intrusion produces strong deformations and lateral displacements. The evidence of a structurally weak zone due to dyke intrusion, combined with our numerical modeling

results, suggests that future large magma upwelling events at Pacaya might strongly destabilize both deep and shallow parts of the cone, particularly in the SW sector. We thus conclude that the development of landslides is a serious threat to the area.

Conclusions

The analysis of the regional tectonic setting, as well as the local structures at Pacaya, suggests that the local stress regime is transtensional with an ENE–WSW σ_3 component. The past history of the edifice sector collapse, the potentially structurally weak zone oriented NNW–SSE, and the recent lava accumulation suggest that the SW flank could be more prone to possible future failures. Limit Equilibrium Method and Finite Element Method analyses of slope stability of the SW flank show that:

- The edifice remains stable under gravity alone;
- A large-scale collapse could be triggered by reasonable ranges of magma pressure (≥ 7.7 MPa if constant along a dyke);
- A peak ground acceleration of ≥ 460 cm/s² could also produce a large lateral failure;
- The pyroclastic deposits beneath the edifice could have influenced the depth and geometry of the ancestral collapse, as the resulting failure surface in the models with a basal pyroclastic layer more closely resembles that of large volcanic landslides documented elsewhere;
- Numerical models reveal that maximum shear strain patterns within the edifice may account for long lava flows erupted from lower vent elevations between 1,600 and 1,800 m asl, as shear fractures can act as conduits for magma to drain out at lower vents.

Acknowledgments This study was performed in the framework of the USA-Italy-France Atlantis INVOGE (International Geologic Masters in Volcanology and Geotechniques) project, and under the umbrella of the International Lithosphere Program–Task Force II. Additionally, this material is based upon work supported by the National Science Foundation under PIRE Grant No. 0530109 and the Michigan Space Grant Consortium. Thank you to Patrick Manzoni for support in the field and laboratory. Special thanks to Sarah Fagents, Lee Siebert, and an anonymous reviewer for their help in improving this manuscript.

References

Álvarez-Gómez JA, Meijer PT, Martínez-Díaz JJ, Capote R (2008) Constraints from finite element modeling on the active tectonics of northern Central America and the Middle America Trench. *Tectonics* 27:1–12

- Apuani T, Corazzato C (2009) Numerical model of the Stromboli volcano (Italy) including the effect of magma pressure in the dyke system. *Rock Mech Rock Eng* 42(1):53–72
- Apuani T, Corazzato C, Cancelli A, Tibaldi A (2005a) Physical and mechanical properties of rock masses at Stromboli: a dataset for volcano instability evaluation. *Bull Eng Geol Environ* 64:419–431
- Apuani T, Corazzato C, Cancelli A, Tibaldi A (2005b) Stability of a collapsing volcano (Stromboli-Italy): limit equilibrium analysis and numerical modelling. *J Volcanol Geotherm Res* 144(1–4):191–210
- Apuani T, Merri A, Masetti M (2007) Effects of volcanic seismic events on the Stromboli stability by finite difference numerical modeling. In: *Proceedings of the International Workshop on Volcanic Rocks*, 11th ISRM Congress. Ponta Delgada, Azores, Portugal, pp. 101–109
- Bardineztzef JM, Deniel C (1992) Magmatic evolution of Pacaya and Cerro Chiquito volcanological complex, Guatemala. *Bull Volcanol* 54:267–283
- Benito MB, Lindholm C, Camacho E, Climent Á, Marroquín G, Molina E, Rojas W, Escobar JJ, Talavera E, Alvarado GE, Torres Y (2012) A new evaluation of seismic hazard for the Central America region. *Bull Seismol Soc Am* 102(2):504–523
- Bieniawski ZT (1989) *Engineering rock mass classifications*. Wiley, New York, p 272
- Bonali F, Corazzato C, Tibaldi A (2011) Identifying rift zones on volcanoes: an example from La Réunion island, Indian Ocean. *Bull Volcanol* 73:347–366
- Borgia A, Ferrari L, Pasquare G (1992) Importance of gravitational spreading in the tectonic and volcanic evolution of Mount Etna. *Nature* 357:231–235
- Burkhardt B, Self S (1985) Extension and rotation of crustal blocks in northern Central America and effect on the volcanic arc. *Geology* 13:22–26
- Caceres D, Monterroso D, Tavakoli B (2005) Crustal deformation in northern Central America. *Tectonophysics* 404:119–131
- Carr M (1976) Underthrusting and Quaternary faulting in northern Central America. *Geol Soc Am Bull* 87:825–829
- Corazzato C, Francalanci L, Menna M, Petrone C, Renzulli A, Tibaldi A, Vezzoli L (2008) What controls sheet intrusion in volcanoes? Petrological and structural characters of the Stromboli sheet complex, Italy. *J Volcanol Geotherm Res* 173:26–54
- del Potro R, Hürlimann M (2008) Geotechnical classification and characterization of materials for stability analyses of large volcanic slopes. *Eng Geo* 98:1–17
- Delcamp A, Wyk V, de Vries B, James MR (2008) The influence of edifice slope and substrata on volcano spreading. *J Volcanol Geotherm Res* 177(4):925–943
- Diñer I, Altay A, Çobanoğlu I, Uras Y (2004) Correlation between Schmidt hardness, uniaxial compressive strength and Young's modulus for andesites, basalts, and tuffs. *Bull Eng Geol Environ* 63:141–148
- Eggers A (1972) *The geology and petrology of the Amatitlán Quadrangle, Guatemala*. PhD Dissertation, Dartmouth College
- Eggers A (1983) Temporal gravity and elevation changes at Pacaya volcano, Guatemala. *J Volcanol Geotherm Res* 19:223–237
- Feldman LH (1993) *Mountains of fire, lands that shake: earthquakes and volcanic eruptions in the historic past of Central America, 1505–1899*. Labyrinthos, Culver City, CA, p. 295
- Franco A, Lasserre C, Lyon-Caen H, Kostoglodov V, Molina E, Guzman-Speziale M, Monterroso D, Robles V, Figueroa C, Amaya W, Barrier E, Chiquin L, Moran S, Flores O, Romero J, Santiago JA, Manea M, Manea VC (2012) Fault kinematics in northern Central America and coupling along the subduction interface of the Cocos Plate, from GPS data in Chiapas (Mexico), Guatemala and El Salvador: kinematics in northern Central America. *Geophys J Int* 189(3):1223–1236

- Frank D (1995) Surficial extent and conceptual model of hydrothermal system at Mount Rainier. Washington. *J Volcanol Geotherm Res* 65:51–80
- Guzman-Speziale M (2001) Active seismic deformation in the grabens of northern Central America and its relationship to the relative motion of the North America-Caribbean plate boundary. *Tectonophysics* 337:39–51
- Hoek E (1994) Strength of rock and rock masses. *ISRM News J* 2(2):4–16
- Hoek E (2007) Practical rock engineering. PDF: www.rocksolid.com/education/hoek_corner. Accessed 8 Aug 2012
- Hoek E, Carranza-Torres C, Corkum B (2002) Hoek-Brown failure criterion—2002 edition. *Proc NARMS-TAC Conf* 1:267–273
- Hungr O, Salgado FM, Byrne M (1989) Evaluation of three-dimensional method of slope stability analysis. *Can Geotech J* 26:679–686
- Hynes ME, Franklin AG (1984) Rationalizing the Seismic Coefficient Method. U.S. Department of the Army. Waterways Experiment Station. US Army Corps of Engineers, Miscellaneous Paper GL-84-13
- IGN, Bonis S (1993) Mapa geológico de Guatemala escala 1:250,000. Hoja ND 15-8-G, “Guatemala”. First edition (map), Guatemala
- IGN, Eggers A (1969) Mapa geológico de Guatemala escala 1:50,000. Hoja 2059 II G, “Amatitlán”. First edition (map), Guatemala
- Iverson R (1995) Can magma-injection and groundwater forces cause massive landslides on Hawaiian volcanoes? *J Volcanol Geotherm Res* 66:295–308
- JICA, INSIVUMEH, SEGEPLAN (2003) Estudio del establecimiento de los mapas básicos de amenaza para el sistema de información geográfica de la República de Guatemala. In: Final report executive abstract (unpublished): 206 p
- Kitamura S, Matías Gómez RO (1995) Tephra stratigraphic approach to the eruptive history of Pacaya volcano, Guatemala. *Science Reports—Tohoku University, Seventh Series. Geography* 45(1):1–41
- Lagmay AMF, Valdivia W (2006) Regional stress influence on the opening direction of crater amphitheatres in Southeast Asian volcanoes. *J Volcanol Geotherm Res* 158:139–150
- Lyon-Caen H, Barrier E, Lasserre C, Franco A, Arzu I, Chiquin L, Chiquin M, Duquesnoy T, Flores O, Galicia O, Luna J, Molina E, Porras O, Requena J, Robles V, Romero J, Wolf R (2006) Kinematics of the North America-Caribbean-Cocos plates in Central America from new GPS measurements across the Polochic-Motagua fault system. *Geophys Res Lett* 33:1–5
- Manzoni P (2012) Slope stability analysis of the Pacaya Volcano, Guatemala, using Limit Equilibrium and Finite Element Method. MS thesis, Michigan Technological University
- Marinos P, Hoek E (2000) GSI—a geologically friendly tool for rock mass strength estimation. In: *Proc. GeoEng 2000 Conference*. Melbourne, Australia, pp. 1422–1442
- Matías Gómez RO (2009) Volcanological map of the 1961–2009 eruption of Volcán de Pacaya, Guatemala. MS thesis, Michigan Technological University
- Matías Gómez RO, Rose WI, Palma JL, Escobar-Wolf R (2012) Notes on a map of the 1961–2010 eruptions of Volcán de Pacaya, Guatemala. *Geol Soc Am Digital Map Chart Series* 10: 10 p
- Merle O, Borgia A (1996) Scaled experiments of volcanic spreading. *J Geophys Res* 101(B6):805–813
- Michalowski RL (2010) Limit analysis and stability charts for 3D slope failures. *J Geotech Geo-Environ Eng* 136:583–593
- Moore JG, Albee WC (1981) Topographic and structural changes, March–July 1980—photogrammetric data. In: Lipman PW, Mullineaux DR (eds). *The 1980 eruptions of Mount St. Helens*, Washington. US Geol Surv Prof Pap 1250: 401–420
- Moriya I (1980) Bandaian eruption and landforms associated with it. In: *Collection of articles in memory of retirement of Prof. K. Hishimura*. Tohoku University, Tokyo:214–219
- Nakamura K (1977) Volcanoes as possible indicators of tectonic stress orientation—principle and proposal. *J Volcanol Geotherm Res* 2(1):1–16
- Nakamura K (1978) Geology and petrology of Bandai and Nekoma volcanoes. *Tohoku Univ Sci Rep* 14:67–119
- Norini G, Acocella V (2011) Analogue modeling of flank instability at Mount Etna: understanding the driving factors. *J Geophys Res* 116(B07206)
- Rocscience (2011) RocLab v1.0, Phase2 v 8.0, Slide v. 6.0. Toronto, Canada
- Rubin AM, Pollard DD (1987) Origin of blade-like dykes in volcanic rift zones. In: Decker RW, Wright TL, Stauffer PH (eds) *Volcanism in Hawaii*. US Geol Surv Prof Pap 1350:1449–1470
- Schaefer LN (2012) Geotechnical data and numerical analysis of edifice collapse and related hazards at Pacaya Volcano, Guatemala. MS thesis, Michigan Technological University
- Siebert L (1984) Large volcanic debris avalanches: characteristics of source areas, deposits, and associated eruptions. *J Volcanol Geotherm Res* 22(3–4):163–197
- Siebert L, Béget JE, Glicken H (1995) The 1883 and late-prehistoric eruptions of Augustine volcano, Alaska. *J Volcanol Geotherm Res* 66:367–395
- Siebert L, Glicken H, Ui T (1987) Volcanic hazards from Bezymianny- and Bandai-type eruptions. *Bull Volcanol* 49(1):435–459
- Siebert L, Alvarado GE, Vallance JW, van Wyk de Vries B (2006) Large-volume volcanic edifice failures in Central America and associated hazards. In: Rose WI, Bluth GJS, Carr MJ, Ewert JW, Patino LC, Vallance JW, (eds) *Volcanic hazards in Central America*. *Geol Soc Am Spec Pap* 412:1–26
- Thomas ME, Petford N, Bromhead EN (2004) Volcanic rock-mass properties from Snowdonia and Tenerife: implications for volcano edifice strength. *J Geol Soc* 161:939–946
- Tibaldi A (2001) Multiple sector collapses at Stromboli Volcano, Italy: how they work. *Bull Volcanol* 63:112–125
- Tibaldi A, Lagmay AMF (2006) Interaction between volcanoes and their basement. *J Volcanol Geotherm Res* 158:1–5
- Tibaldi A, Rust D, Corazzato C, Merri A (2010) Setting the scene for self-destruction: From sheet intrusions to the structural evolution of rifted stratovolcanoes. *Geosphere* 6(3):189–210
- Ui T, Yamamoto H, Suzuki K (1986) Characterization of debris avalanche deposits in Japan. *J Volcanol Geotherm Res* 29:231–243
- Vallance JW, Siebert L, Rose WI, Raul Giron J, Banks NG (1995) Edifice collapse and related hazards in Guatemala. *J Volcanol Geotherm Res* 66:337–355
- Voight B, Elsworth D (1997) Failure of volcano slopes. *Geotechnique* 47(1):1–31
- Walker JA (1989) Caribbean arc tholeiites. *J Geophys Res* 94:10539–10548
- Wooller L, Wyk V, de Vries B, Murray JB, Rymer H, Meyer S (2004) Volcano spreading controlled by dipping substrata. *Geology* 32:573–576
- Wunderman RL, Rose WI (1984) Amatitlán, an actively resurging cauldron 10 km south of Guatemala City. *J Geophys Res* 89:8525–8539